Eur. Phys. J. E (2016) **39**: 92
DOI 10.1140/epje/i2016-16092-7

THE EUROPEAN PHYSICAL JOURNAL E

Regular Article

On the morphological stability of multicellular tumour spheroids growing in porous media

Chiara Giverso[1] and Pasquale Ciarletta[1,2,a]

[1] Dipartimento di Matematica - MOX, Politecnico di Milano, Piazza Leonardo da Vinci, 32 - 20133 Milano, Italy
[2] CNRS and Sorbonne Universités, UPMC Univ Paris 06, UMR 7190, Institut Jean le Rond d'Alembert, 4 place Jussieu case 162, 75005 Paris, France

Received 31 May 2016 and Received in final form 6 September 2016
Published online: 12 October 2016 –

Abstract. Multicellular tumour spheroids (MCTSs) are extensively used as *in vitro* system models for investigating the avascular growth phase of solid tumours. In this work, we propose a continuous growth model of heterogeneous MCTSs within a porous material, taking into account a diffusing nutrient from the surrounding material directing both the proliferation rate and the mobility of tumour cells. At the time scale of interest, the MCTS behaves as an incompressible viscous fluid expanding inside a porous medium. The cell motion and proliferation rate are modelled using a non-convective chemotactic mass flux, driving the cell expansion in the direction of the external nutrients' source. At the early stages, the growth dynamics is derived by solving the quasi-stationary problem, obtaining an initial exponential growth followed by an almost linear regime, in accordance with experimental observations. We also perform a linear-stability analysis of the quasi-static solution in order to investigate the morphological stability of the radially symmetric growth pattern. We show that mechano-biological cues, as well as geometric effects related to the size of the MCTS subdomains with respect to the diffusion length of the nutrient, can drive a morphological transition to fingered structures, thus triggering the formation of complex shapes that might promote tumour invasiveness. The results also point out the formation of a retrograde flow in the MCTS close to the regions where protrusions form, that could describe the initial dynamics of metastasis detachment from the *in vivo* tumour mass. In conclusion, the results of the proposed model demonstrate that the integration of mathematical tools in biological research could be crucial for better understanding the tumour's ability to invade its host environment.

1 Introduction

A multicellular tumour spheroid (MCTS) is an ensemble of tumour cells organized in a multi-layered structure [1,2]. In general, a MCTS consists of a central core of necrotic cells, surrounded by a layer of quiescent (*i.e.* dormant) cells and an outer rim of proliferating cells [1–4].

MCTSs are widely used *in vitro* to study the early stages of avascular tumour growth and to assess the efficacy of anti-cancer drugs and therapies, since their growth and structure resemble the *in vivo* avascular phase of solid tumour invasion. Such an early growth phase is characterized by diffusion-limited growth, since the tumour absorbs vital nutrients via diffusion from the external environment [1, 3, 5]. Thus, diffusion may become suddenly ineffective in the center of the tumour mass, forming a characteristic necrotic core (see fig. 1a). At later stages, a solid tumour is characterized by the occurrence of angiogenesis (*i.e.* the process by which the tumour induces new blood vessels formation from the nearby existing vasculature), thus switching to a vascular growth phase [6, 7].

The analysis of the avascular growth phase in tumours has attracted a lot of interest in the mathematical and physical research communities, and a large number of *in silico* mathematical models has been proposed [2, 8–16]. Thanks to the controllability and the reproducibility of the experimental setting, MCTS has become a widely used system model for the development of theoretical models.

The classical approach of deterministic tumour model comprised an ordinary differential equation (ODE), derived from either mass conservation or population dynamics, coupled with at least one reaction-diffusion equation, representing the spatio-temporal distribution of vital nutrients or chemical signals inside the tumour [2, 9–12, 14, 15, 17]. Only recently, many authors have extended such models including the pivotal role of mechanics in tumour growth. In most cases, fluid-like constitutive equations have been used to model the tumour mass [18–26]. This choice is obviously only an approximation of the by far more complex behaviour of cellular aggregates, that

[a] e-mail: pasquale.ciarletta@polimi.it

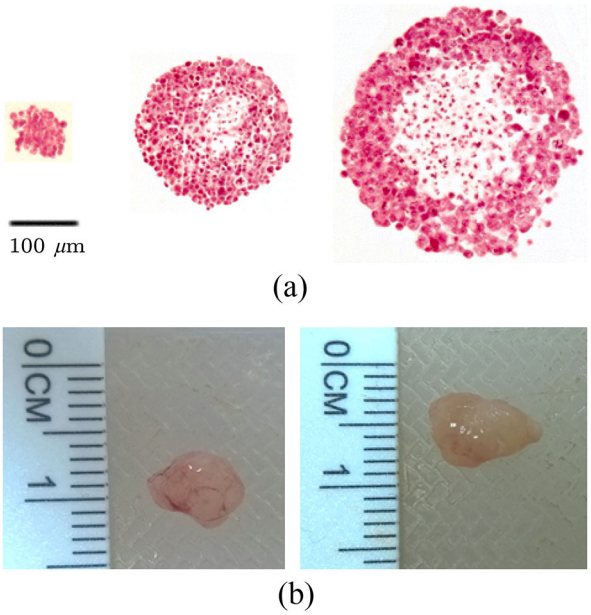

Fig. 1. (a) Morphological evolution of a multicellular tumour spheroid of HeLa cells, showing the development of an undulated contour and a necrotic core (reproduced with permission from [51]). HeLa cells were trypsinized, counted and grown as multicellular spheroids using the liquid overlay technique. The sections were counterstained with hematoxylin and eosin to visualize the cytoplasms of the cells. The multicellular spheroid section is reproduced at days 0, 4 and 12, from left to right. (b) Solid tumours extracted from mice after orthotopic implant of MCF10CA1a cell lines in the mammary fat pad of the nude mice (courtesy of T. Stylianopoulos, Cancer Biophysics Laboratory, University of Cyprus).

also display solid-like properties related to the adhesive characteristics of cells [27] and to the mechanical properties of the single cell in the cluster. Thus, in some limiting cases, cell aggregates are better described as solids with linear or eventually nonlinear elasticity, in which compressive and shear loads are balanced by the solid stress in the body, depending on the strain of its material points [28–33]. A solid-like constitutive equation has been advocated for its suitability of accounting for both residual stresses [29, 32, 34] and the plastic behaviour of cellular aggregates [35–37]. Even though these considerations support the idea that a cellular aggregate can behave as a solid at some extent, experimental evidences [26, 38, 39] have shown that aggregates behave as elastic solids on short timescales (of the order of a few minutes) but display a fluid-like behaviour at longer times. Furthermore, it was shown that cellular aggregates behave as an elastic solids at time scales short compared to that of cell division and apoptosis, and as a fluid (with the traceless stress that relaxes to zero) for long times [40]. Thus the description of MCTSs as a liquid is widespread.

Even though the existing mathematical models on both solid tumours and MCTSs successfully reproduce the experimentally observed growth dynamics [2, 9–12, 14, 15, 17, 41, 42], they poorly consider the mechanical and chemical interaction with the surrounding environment. Furthermore, most approaches assume that the initial spherical symmetry is preserved during the growth of the aggregate [28–30], whilst only in few cases [11, 12, 15] the development of tumour irregular contours has been taken into account. Indeed, it is known that some solid tumours, *e.g.* carcinomas, grow almost spherically only in the first stages of their progression [1,3,5], while they might show a less defined and even asymmetric outer boundary [43] (see fig. 1b). Since higher irregular contours usually indicate aggressive tumours, the capability to undergo a morphological transition might promote tumour infiltration and invasion within the surrounding tissue [2,11,12,15,44–46]. Thus, it has been proposed that some measure of the irregularity of a tumour boundary (*e.g.* its fractal index measured via particular medical imaging techniques such as computerized tomography scans), may provide clinicians with useful information for its prognosis and treatment [44–46], being potentially useful in predicting the efficacy of drug treatment or chemotherapy [47, 48].

In this work we go beyond the state-of-the art in the field [2, 49, 50] by proposing a mathematical model that accounts for the presence of a surrounding porous media with a finite thickness. Thus, nutrient diffusion from the external environment creates a chemical gradient that directs both the proliferation rate and the motility of the tumour cells. MCTS is modelled as a viscous fluid with adhesive interactions at the border, expanding inside a porous material.

This work is organized as follows. First, we introduce in sect. 2 the mathematical model describing the expansion of an initially spherical tumour. In sect. 3, we derive the radially symmetric solution of the quasi-stationary problem. Then, we perform a linear stability on the quasi-static tumour growth. Finally, in sect. 4, we discuss the modelling results with respect to the key chemo-mechanical and geometric parameters that govern the mathematical problems, highlighting the key mechano-biology effects that promote a morphological transition during tumour invasion.

2 Mathematical model

The MCTS is modelled as a three-dimensional continuum growing inside a rigid porous structure, representing the surrounding environment, usually extracellular matrix (ECM) or matrigel. In this respect, the proposed model refers to the *in vitro* case in which MCTS grows inside a three-dimensional either natural medium (*e.g.* agarose gel, hyaluronic acid gel) or synthetic matrices scaffolds (*e.g.* polylactide and polyglycolide biodegradable structures mimicking a tissue-like environment) [52].

The outer boundary of the tumour is considered as a freely moving material interface separating the tumour cells from the surrounding medium.

In particular, we account for the presence of a central region of necrotic cells, surrounded by a layer of quiescent and proliferating cells. Thus, the whole domain Ω

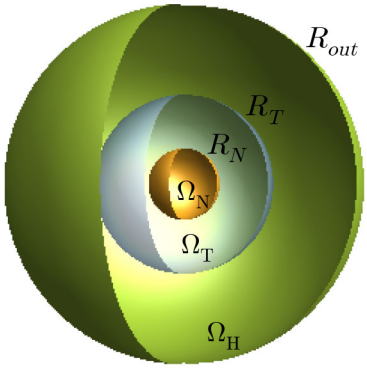

Fig. 2. Representation of the domain used for the analytical analysis. At time $t = 0$, the three domains Ω_N, Ω_T and Ω_H are concentric spherical shells, with radius R_N, R_T and R_{out}, respectively. In this work, we consider that only the tumour boundary $\partial\Omega_T$ evolves in time.

is divided in different regions, depending on the residing cellular population (see fig. 2):

– the necrotic cells are located in the central core of the spheroid, in a region called $\Omega_N(t)$, with

$$\Omega_N(t)=\{(r,\theta) : r < R_N(t),\ 0 < \varphi \leq \pi,\ 0 < \theta \leq 2\pi\},$$

where R_N is the radius of the necrotic core, that might evolve in time;

– the proliferative and quiescent tumour cells are located in the region

$$\Omega_T(t) = \{(r,\theta) : R_N(t) < r < R_T(t),\ 0 < \varphi \leq \pi,\ 0 < \theta \leq 2\pi\},$$

where R_T is the radius of the spheroid, whose evolution in time represents the growth of the MCTS;

– the healthy space, composed by either the *in vitro* scaffold or the extracellular matrix, the extracellular liquid and possibly healthy cells (*in vivo*),

$$\Omega_H(t) = \{(r,\theta) : R_T(t) < r < R_{\text{out}},\ 0 < \varphi \leq \pi,\ 0 < \theta \leq 2\pi\},$$

being R_{out} the outer boundary of the whole domain.

The boundary between the necrotic core and the proliferative region is called $\partial\Omega_N(t)$, whereas the moving interface between the tumour region and the healthy space is denoted with $\partial\Omega_T(t)$. In the following we will consider that the interior boundary between the necrotic core and the quiescent-proliferative region does not evolve in time, since we are interested only in the evolution of the MCTS boundary, which is related to tumour infiltration inside the healthy region. Furthermore, we assume that the porous material is homogeneously distributed in the whole region $\Omega = \Omega_N \cup \Omega_T(t) \cup \Omega_H(t)$ and it is neither produced/degraded (*i.e.* behaves as inert matter), nor deformed (*i.e.* structurally rigid) by the moving tumour cells. We will consider a single nutrient species (*e.g.* oxygen) with volume concentration $n(\mathbf{x}, t)$, diffusing from the fixed outer boundary $\partial\Omega$ through the porous material. Thus, we assume that the vascular network providing the source of nutrients is outside the modelled domain, and can be represented by a boundary term at $\partial\Omega$. The diffusion coefficient is a constant value D_n everywhere, but the nutrient is only consumed, with an uptake rate γ_n, in the region occupied by the proliferative and quiescent cells. Indeed we consider that the consumption of nutrients in the healthy region is negligible. This is certainly the case of MCTSs growing inside artificial/natural scaffolds, but, in a first approximation, it can be used also to model the *in vivo* condition [20, 53], since the net consumption of nutrients in the extracellular healthy space is negligible compared to the uptake by tumour cells [54].

Thus, the 3D homogenized concentration per unit volume of this generic chemical species, indicated with $n(\mathbf{x}, t)$, obeys the following reaction-diffusion equation:

$$\dot{n}(\mathbf{x},t) = \begin{cases} D_n\nabla^2 n(\mathbf{x},t) & \text{in } \Omega_N, \\ D_n\nabla^2 n(\mathbf{x},t) - \gamma_n n(\mathbf{x},t) & \text{in } \Omega_T(t), \\ D_n\nabla^2 n(\mathbf{x},t) & \text{in } \Omega_H(t). \end{cases} \quad (1)$$

We remark that, in principle, the uptake rate γ_n should depend on the tumour cell density, although, in the following, it will be considered homogeneous and constant over time. Even the diffusion coefficient D_n can be affected by the cell packing inside the tumour and by the extracellular matrix alignment and distribution. However, coherently with the hypothesis of an inert, rigid and homogeneous extracellular matrix distributed in the whole domain, the diffusion of nutrients can be assumed to be constant [53, 55].

The diffusing nutrient notably not only affects the growth of single individuals in the tumour but also directs cell movements, *e.g.* through chemotaxis [56, 57]. Therefore, we consider a non-convective mass flux term, $\mathbf{m}$, taking into account both tumour proliferation and chemotactic motion, differently from the standard volumetric production rate considered in literature [2, 11–15]. Accordingly, the mass balance inside $\Omega_T(t)$ reads

$$\frac{\mathrm{d}\rho}{\mathrm{d}t} + \rho\nabla\cdot\mathbf{v} = \nabla\cdot\mathbf{m} \quad \text{in } \Omega_T(t), \quad (2)$$

where ρ is the tumour cell density, which is approximately the same of water. Since mass transport phenomena in MCTSs are driven by the local concentration of chemicals, the mass flux vector appearing in eq. (2) should depend on nutrient availability. A simple constitutive law for $\mathbf{m}$ can be taken in the form of a chemotactic term [56, 58], *i.e.* $\mathbf{m} = \chi\rho\nabla n$, where χ is the chemotactic coefficient, here considered constant. Consequently, the mass flux $\mathbf{m}$ describes the expansion of the tumour due to proliferation and driven by chemotaxis towards higher concentration of nutrients.

Assuming that the living aggregate can be macroscopically modelled as a Newtonian fluid, Darcy's law describes its motion inside the inert, porous surrounding

medium [2,18]. Thus, the cell velocity $\mathbf{v}$ is related to the pressure field p through

$$\mathbf{v} = -K_p \nabla p, \tag{3}$$

where K_p is related to the permeability of the medium, k, and the viscosity of the cellular material, μ, by $K_p = k/\mu$. Assuming the incompressibility of the cellular spheroid, which is mostly composed by water, we impose $\mathrm{d}\rho/\mathrm{d}t = 0$ in eq. (2), so that the relation between the pressure p and the nutrient concentration n reads

$$\nabla^2 p = -\frac{\chi}{K_p}\nabla^2 n \quad \text{in } \Omega_T(t), \tag{4}$$

which has been obtained substituting the Darcy's law (3) and the constitutive relations for $\mathbf{m}$ in the mass balance equation (2). In summary, the coupling of eq. (1) with eq. (4), complemented by a proper set of boundary conditions (BCs), describes the macroscopic evolution of the avascular tumour inside the healthy tissue.

In particular, for the pressure we impose the Young-Laplace equation at the moving boundary $\partial\Omega_T(t)$ and the null velocity of the tumour cells at the fixed boundary $\partial\Omega_N$, *i.e.*

$$p = p_0 - \sigma_b C \quad \text{on } \partial\Omega_T(t), \tag{5}$$

$$\mathbf{v}_{\partial\Omega_N}\cdot\mathbf{n}_N = 0 \rightarrow (\nabla p)|_{\partial\Omega_N}\cdot\mathbf{n}_N = 0 \quad \text{on } \partial\Omega_N, \tag{6}$$

being $\mathbf{n}_N$ the normal at the fixed boundary $\partial\Omega_N$, C the local curvature of the free boundary $\partial\Omega_T(t)$, p_0 the constant pressure in the outer healthy domain and σ_b the surface tension at the moving interface. The surface tension σ_b arises from the collective adhesive interaction among tumour cells at the MCTS boundary, primarily mediated by cadherins, [59] and from the differential contractility between the cell-cell and cell-medium interfaces, mainly mediated by α-catenin [60]. Even if, in principle the surface tension σ_b depends on the density of cells, the distribution of cadherins and the presence of α-catenin [60], we will assume that it can be considered constant, for the chosen cellular population composing the aggregate.

For what concerns the chemical species, in absence of an interfacial structure, the continuity for the nutrient concentration and flux can be imposed (both in $\partial\Omega_T(t)$ and in $\partial\Omega_N$), and the concentration at the outer boundary can be assumed constant (to model the source of nutrients from the external vascular network), so that

$$n|_{\partial\Omega} = n_{\text{out}} \quad \text{on } \partial\Omega, \tag{7}$$

$$[\![n]\!]|_{\partial\Omega_T} = 0, \quad [\![\nabla n]\!]|_{\partial\Omega_T}\cdot\mathbf{n} = 0 \quad \text{on } \partial\Omega_T, \tag{8}$$

$$[\![n]\!]|_{\partial\Omega_N} = 0, \quad [\![\nabla n]\!]|_{\partial\Omega_N}\cdot\mathbf{n}_N = 0 \quad \text{on } \partial\Omega_N, \tag{9}$$

where $\mathbf{n}$ is the outward normal vector at the boundary $\partial\Omega_T$ and $[\![(\cdot)]\!]|_{\partial\Omega_j}$ denotes the jump of the quantity between brackets across the boundary $\partial\Omega_j$, with $j = N, T$.

Finally, the compatibility condition at the free interface imposes

$$\frac{\mathrm{d}\mathbf{x}_{\partial\Omega_T}}{\mathrm{d}t}\cdot\mathbf{n} = \mathbf{v}_{\partial\Omega_T}\cdot\mathbf{n} \quad \text{on } \partial\Omega_T. \tag{10}$$

In the following we will work with dimensionless equations, obtained writing the system of eqs. (1)–(4) in terms of the dimensionless chemical concentration, $\bar{n} = n/n_c$, and the dimensionless pressure, $\bar{p} = p/p_c$ and referring to the geometry outlined in fig. 2. The dimensionless quantities are obtained using the following characteristic time t_c, length l_c, velocity v_c, pressure p_c and chemical concentration n_c: $t_c = \gamma_n^{-1}$, $l_c = \sqrt{D_n\gamma_n^{-1}}$, $v_c = \sqrt{D_n\gamma_n}$, $p_c = D_n K_p^{-1}$, $n_c = n_{\text{out}}$. Finally, the resulting dimensionless systems of equations reads

$$\dot{\bar{n}} = \begin{cases} \bar{\nabla}^2\bar{n} & \text{for } \bar{r} < \bar{R}_N, \\ \bar{\nabla}^2\bar{n} - \bar{n} & \text{for } \bar{R}_N < \bar{r} < \bar{R}_T(t), \\ \bar{\nabla}^2\bar{n} & \text{for } \bar{R}_T(t) < \bar{r} < \bar{R}_{\text{out}} \end{cases} \tag{11a}$$

$$\bar{\nabla}^2\bar{p} = -\beta\bar{\nabla}^2\bar{n} \quad \text{for } \bar{R}_N < \bar{r} < \bar{R}_T(t), \tag{11b}$$

$$[\![\bar{n}]\!]|_{\bar{R}_N} = 0, \quad [\![\bar{\nabla}\bar{n}]\!]|_{\bar{R}_N}\cdot\bar{\mathbf{n}}_N = 0, \quad (\bar{\nabla}\bar{p})\cdot\bar{\mathbf{n}}_N = 0 \quad \text{for } \bar{r} = \bar{R}_N, \tag{11c}$$

$$[\![\bar{n}]\!]|_{\bar{R}_T} = 0, \quad [\![\bar{\nabla}\bar{n}]\!]|_{\bar{R}_T}\cdot\bar{\mathbf{n}} = 0, \quad \bar{p} = \bar{p}_0 - \bar{\sigma}\bar{C} \quad \text{for } \bar{r} = \bar{R}_T(t), \tag{11d}$$

$$\bar{n}(\bar{t}, \bar{R}_{\text{out}}) = 1 \quad \text{for } \bar{r} = \bar{R}_{\text{out}}, \tag{11e}$$

$$\frac{\mathrm{d}\bar{\mathbf{x}}_{\bar{R}_T}}{\mathrm{d}\bar{t}}\cdot\bar{\mathbf{n}} = \bar{\mathbf{v}}_{\bar{R}_T}\cdot\bar{\mathbf{n}} = -\bar{\nabla}\bar{p}|_{\bar{R}_T}\cdot\bar{\mathbf{n}} \quad \text{for } \bar{r} = \bar{R}_T(t). \tag{11f}$$

The non-dimensionalization leads to the definition of five dimensionless parameters, classified into two broad categories:

- $\beta := \chi n_c/D_n$ and $\sigma := \sigma_b K_p \gamma_n^{1/2} D_n^{-3/2} = \sigma_b K_p l_c^{-1/2} D_n^{-1}$ define mechano-biology effect on the aggregate expansion, and are called *motility* parameters;
- $\bar{R}_N$, $\bar{R}_T$ and $\bar{R}_{\text{out}}$ (*i.e.* the dimensionless radii of the necrotic core, of the MCTS and the whole domain, respectively) define the geometrical properties of the system with respect to the diffusive length l_c, and are denoted as *size* parameters.

In particular, the dimensionless parameter β represents the chemical effects associated to the expansion of MCTSs, since it can be regarded as the ratio between the typical time-scales of mass production over nutrient diffusion. On the other hand, the parameter σ defines the influence of mechanical cues over tumour development, representing the ratio of the surface tension of the aggregate over the characteristic viscous pressure of the fluid ensemble.

For sake of simplicity, in the following we will omit the barred notation to denote dimensionless quantities, *e.g.* R_T stands for $\bar{R}_T$ and so on.

$$n^* = \begin{cases} \dfrac{2R_{\rm out}e^{R_T+R_N}}{e^{2R_T}w_T^+ - e^{2R_N}w_T^-} & \text{if } r \le R_N \\ -\dfrac{e^{2R_N}[e^{2(r-R_N)}(R_N+1)R_{\rm out} + (R_N-1)R_{\rm out}]}{rw_T^- e^{r-R_T+2R_N} - rw_T^+ e^{r+R_T}} & \text{if } R_N < r \le R_T \\ \dfrac{R_{\rm out}[e^{2R_T}(R_N+1)(r-R_T+1) - e^{2R_N}(R_N-1)(r-R_T-1)]}{r(e^{2R_T}w_T^+ - e^{2R_N}w_T^-)} & \text{otherwise} \end{cases} \tag{12}$$

$$p^* = p_0 + \frac{\sigma}{R_T} + \beta(n^*_{R_T} - n^*) \tag{13}$$

3 Linear-stability analysis of the quasi-static solution

In this section, we first derive the quasi-static solution of the proposed model in order to mimic the early avascular growth. We later perform a linear-stability analysis to investigate the occurrence of a morphological instability at later growth stages.

3.1 Quasi-stationary solution

At early stages of avascular growth MCTSs maintain a spherical shape [1, 3, 5]. Thus, we look for a radially symmetric quasi-stationary solution, assuming that the diffusive process is much faster than the MCTS expansion, so that it is possible to drop the time derivative in eq. (11a). This assumption is valid in many biological conditions, since a fast-growing tumour may expand at a rate of up to 0.5 mm/day, whereas a typical diffusion time scale is about 1 min (considering a typical length scale $L \approx 10^{-2}$ cm and a typical diffusion coefficient $D \approx 10^{-6}\,\mathrm{cm^2\,s^{-1}}$) [11]. Thus, it is clear that the diffusion timescale of nutrients is much shorter than the growth timescale, so that the quasi-stationary assumption can be effectively formulated. Furthermore for such long time scale the MSC can be actually treated as a viscous fluid.

Specializing our analysis to the case of a spherical tumour of radius R_T, we will denote with $n^* = n^*(r,t)$ the quasi-stationary solution of eq. (11a) and with $p^* = p^*(r,t)$ the quasi-stationary pressure field satisfying (11b). Given the boundary conditions (11c)-(11d)-(11e) and considering that n^* and p^* should be bounded, the quasi-stationary fields read

see eqs. (12) *and* (13) *above*

where we called $n^*_{R_T} = n^*(R_T)$ the concentration of the nutrient at the boundary of the aggregate and we defined $w_T^+ = (R_N+1)(R_{\rm out}-R_T+1)$ and $w_T^- = (R_N-1)(R_{\rm out}-R_T-1)$, being $w_T = (R_{\rm out}-R_T)$ the width of the region occupied by the tumour. Then, using eq. (11f), it is possible to compute the quasi-stationary velocity of the front, which is directed along the radial direction for symmetry considerations, *i.e.* $\mathbf{v}^* = v_r^*\mathbf{e}_r$, with

$$v_r^*(R_T) = \beta\,\frac{R_{\rm out}\left(e^{2R_N}(R_N-1)(R_T+1) - e^{2R_T}(R_N+1)(R_T-1)\right)}{R_T^2\left(e^{2R_N}w_T^- - e^{2R_T}w_T^+\right)}\,. \tag{14}$$

Equation (14) can be integrated numerically to determine the evolution of the spheroid border over time. The result, reported in fig. 3 for different values of the parameter β, highlights the existence of an initial phase in which the growth of the aggregate is nearly exponential and a subsequent one in which the expansion of the tumour is almost linear, as observed in [32, 61]. Indeed, in standard MCTS free-growth (*i.e.* without the introduction of an external stress) in liquid suspension or at moderate agarosis gel concentration, the plot of the tumour diameter over time exhibits an early stage of exponential growth, corresponding to spheroid volumetric growth, since nutrients are available everywhere in the spheroid bulk [32,61]. Subsequently, when the diameter of the spheroid becomes much larger than the penetration length of the nutrient, the cellular growth becomes mainly localized on the surface of the tumour, leading to a linear growth in time.

3.2 Perturbation of the quasi-stationary solution

In this section, we investigate the stability of the steady, radially symmetric solution by applying small perturbations of the MCTS boundary.

Let R_T^* be the unperturbed position of the moving interface, we consider a small perturbation ($\varepsilon \ll 1$) of the kind

$$R(\theta,\varphi,t) = R_T^*(t) + \varepsilon e^{\lambda t}\mathbb{R}\mathrm{e}\left[Y_\ell^m(\theta,\varphi)\right], \tag{15}$$

where $\lambda \in \mathbb{R}$ is the *amplification rate* (or *time-growth rate*) of the perturbation and $Y_\ell^m(\theta,\varphi)$ is the spherical harmonic of *degree* ℓ and *order* m, with $m \in \mathbb{N}$, $\ell \in \mathbb{N}^+$ and $|m| \le \ell$. The spherical harmonics $Y_\ell^m(\theta,\varphi)$ form a complete set of orthonormal functions and thus any square-integrable function can be expanded as a linear combination of spherical harmonics. For physical consistency, the variations of n and p from the quasi-stationary solutions n^* and p^*

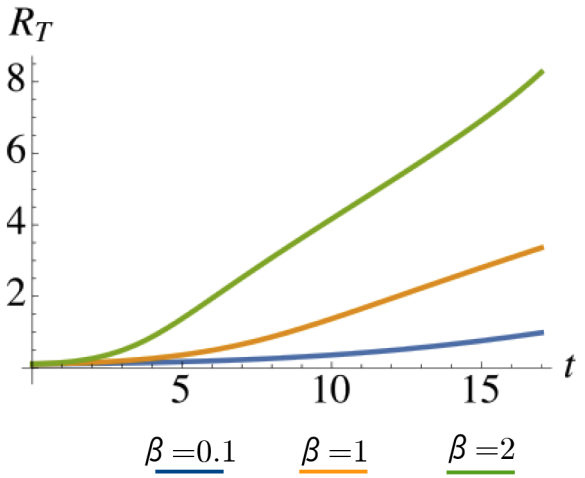

Fig. 3. Quasi-stationary solution of the proposed model, depicting the radius of the tumour over time for different values of the motility parameter β. At early stages the growth is exponential, as a consequence of the bulk availability of nutrients. At later stages, the growth law is almost linear, reflecting the higher nutrient concentration on the outer surface of the growing spheroid.

should be in the form

$$n(r,\theta,\varphi,t) = n^*(r,t) + \varepsilon n_1(r) e^{\lambda t} \mathbb{R}\mathrm{e}\left[Y_\ell^m(\theta,\varphi)\right], \quad (16)$$

$$p(r,\theta,\varphi,t) = p^*(r,t) + \varepsilon p_1(r) e^{\lambda t} \mathbb{R}\mathrm{e}\left[Y_\ell^m(\theta,\varphi)\right]. \quad (17)$$

Using eq. (11a) and the relation $\nabla^2_\Omega Y_\ell^m + \ell(\ell+1)Y_\ell^m = 0$, where we set the angular part of the Laplacian operator as $\nabla^2_\Omega(\cdot) = 1/\sin\theta\,\partial/\partial\theta(\sin\theta\,\partial(\cdot)/\partial\theta) + 1/\sin^2\theta\,\partial^2(\cdot)/\partial\phi^2$, the term n_1 must obey the following ODE:

$$r^2 n_1''(r) + 2r n_1'(r) - \left(\ell(\ell+1) + (\lambda + \mathbf{1}_{\Omega_T} r^2\right) n_1(r) = 0, \quad (18)$$

where primes denote derivatives on r and $\mathbf{1}_{\Omega_T} = 1$ if $R_N < r \leq R_T^*$, $\mathbf{1}_{\Omega_T} = 0$ otherwise. The solution of eq. (18), for $\lambda \neq \{0, -1\}$ is

$$n_1(r) = \begin{cases} C_1 i_\ell\left(\sqrt{\lambda} r\right) & \text{if } r \leq R_N, \\ B_1 i_\ell\left(\sqrt{\lambda+1} r\right) + B_2 k_\ell\left(\sqrt{\lambda+1} r\right) & \text{if } R_N < r \leq R_T^*, \\ A_1 i_\ell\left(\sqrt{\lambda+1} r\right) + A_2 k_\ell\left(\sqrt{\lambda+1} r\right) & \text{if } R_T^* < r \leq R_{\text{out}}, \end{cases} \quad (19)$$

where $i_\ell(r)$ and $k_\ell(r)$ are the modified spherical Bessel function of the first and second kind, respectively, evaluated in r. The coefficients A_1, A_2, B_1, B_2, C_1 appearing in the expression of $n_1(r)$ can be determined imposing the incremental boundary conditions for the concentration field (11c), (11d) and (11e), being

$$[\![n_1]\!]|_{R_N} = 0, \qquad \left[\!\left[\frac{\partial n_1}{\partial r}\right]\!\right]\Big|_{R_N} = 0, \quad (20)$$

$$[\![n_1]\!]|_{R_T^*} = 0, \qquad \left[\!\left[\frac{\partial n_1}{\partial r}\right]\!\right]\Big|_{R_T^*} = n_0, \quad n_1(R_{\text{out}}) = 0. \quad (21)$$

The perturbed pressure field p_1 in Ω_T is obtained from eq. (11b) that leads to

$$p_1(r) = Q r^\ell + W r^{-\ell-1} - \beta\left(B_1 i_\ell\left(\sqrt{\lambda+1} r\right) + B_2 k_\ell\left(\sqrt{\lambda+1} r\right)\right), \quad (22)$$

where the constants Q and W can be determined from the boundary conditions on the pressure field (11c) and (11d), considering only the first order terms, *i.e.*

$$p_1(R_T^*) = -\sigma \frac{2}{{R_T^*}^2}\left(2 - (\ell+1)\ell\right) - \left.\frac{\partial p^*}{\partial r}\right|_{R_T^*},$$
$$\left.\frac{\partial p_1}{\partial r}\right|_{R_N} = 0. \quad (23)$$

Finally, using standard procedures in perturbation theory [62], imposing the boundary condition (10) at the perturbed interface and neglecting the terms of order higher than the first in the series expansion, it is possible to obtain the following dispersion equation

$$\lambda = -p^{*\prime\prime}(R_T^*) - p_1'(R_T^*), \quad (24)$$

which has the same form of the relation found for the rectilinear front on an infinite domain [63] or an expanding circular colony [64, 65]. The dispersion equation (24) is an implicit function of the time-growth mode λ and the spherical harmonic degree ℓ, depending on the five dimensionless parameters β_i, σ, R_N, R_T^* and R_{out}. Interestingly, λ does not depend on the azimuthal component of the model solutions $Y_\ell^m(\phi,\theta)$, *i.e.* the solutions are independent of the order m, as observed also in previous works based on different models [15, 50].

4 Results and discussion

The dispersion equation (24) has been solved numerically in order to investigate the global stability of the solutions depending on the system parameters. The corresponding dispersion diagrams are reported in fig. 4 for different values of both the size and the motility parameters. As in classical perturbation theory [62], a positive real part of the growth rate λ implies global instability, thus highlight a critical spatial mode of the perturbation defined by the degree ℓ associated with the highest positive growth rate. Interestingly, fig. 4 shows that the spheroid front is linearly unstable at small ℓ, with $\ell = 1$ being always unstable. Indeed, whilst for a spheroid growing inside an infinite homogeneous domain with constant chemical concentration, one would expect to find $\lambda = 0$ for $\ell = 1$, due to translational symmetry [11, 15, 50], we must remind that in our case, due to the presence of the external environment the translational symmetry is no longer preserved.

Furthermore, the dispersion diagrams in fig. 4 also indicate the emergence of a characteristic mode different from $\ell = 1$ in the cases of bigger size parameters (see fig. 4a), as well as of small values of the motility parameters σ (see fig. 4c) and β (see fig. 4d). Interestingly, the

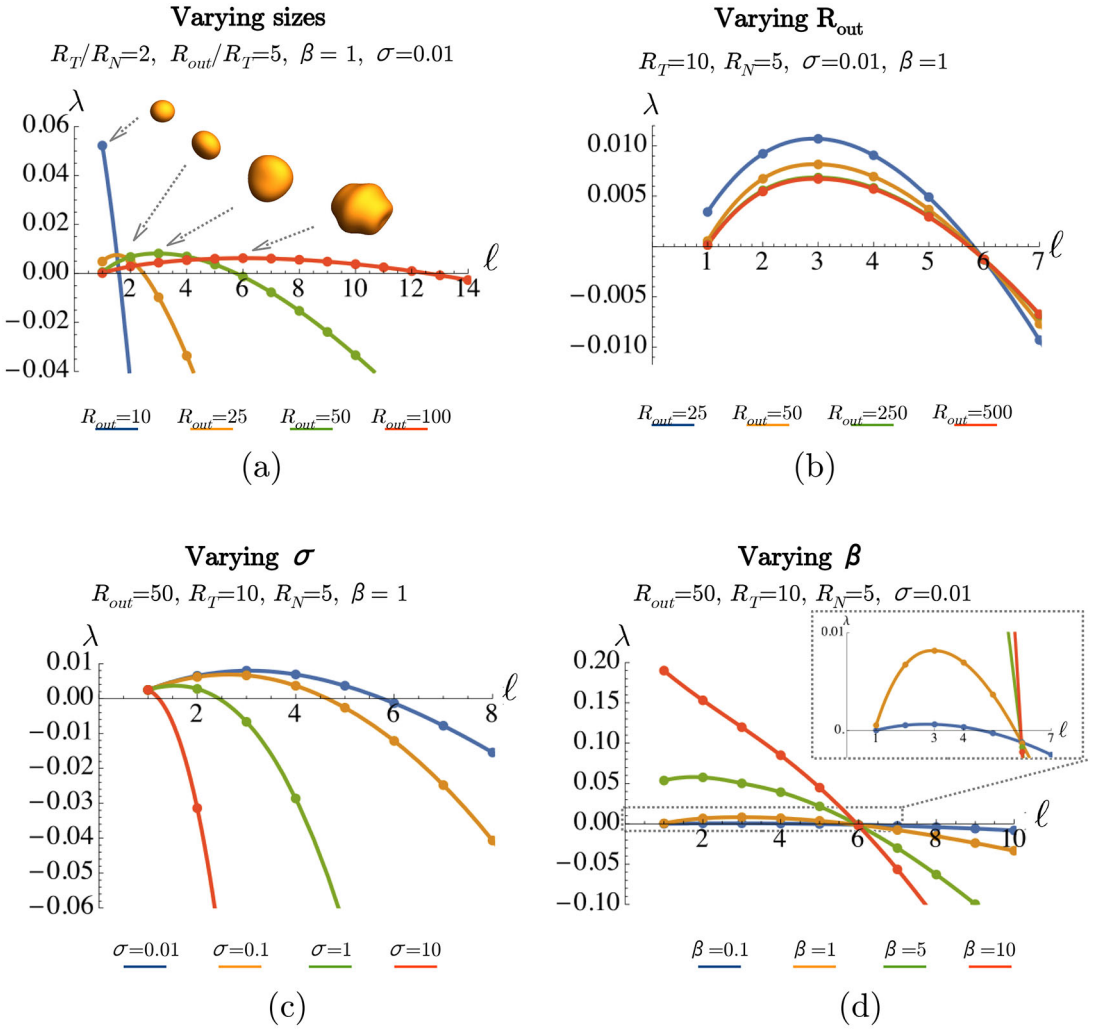

Fig. 4. Dispersion diagrams for different values of the model parameters (a) R_{out} keeping $q = R_{\text{out}}/R_N$ constant, (b) R_{out} keeping R_N constant, (c) σ and (d) β. The solid lines in the graphs are obtained by interpolating the discrete values (see the dots on the curves) of the time growth rate of the perturbation, λ, calculated for integer values of ℓ from eq. (24). In (a) the shapes of the tumour corresponding to the characteristic mode ($\ell = 1, 2, 3, 6$) are reported.

characteristic mode is not significantly affected by varying only the dimension of the external domain, while keeping the necrotic radius R_N and the initial tumour radius R_T fixed (fig. 4b) Moreover, whether the range of unstable modes is highly influenced by the sizes parameters and by the motility parameter σ (fig. 4a-c), it is not deeply influenced by variations of R_{out} and β (fig. 4b-d). Indeed as either the size of the domains decreases (fig. 4a) or σ increases, the range of unstable modes decreases, up to a range where only $\ell = 1$ is unstable. The dependency on the size of the domains states that smaller diffusive lengths (*i.e.* smaller diffusion coefficient or higher absorption rate of the nutrients) lead to highly irregular contours during the growth of the tumour. On the other hand, the effect on the mechanical parameter σ on the dispersion diagram shows that, as expected, the surface tension σ_b, along with a high permeability of the surrounding porous environment k act a stabilizing effect on the front (see fig. 4c), whereas the viscosity of the tumour cluster destabilizes the border of the MCTS leading to more aggressive tumours. As β settles the velocity of the quasi-stationary moving front (see eq. (14)), the dispersion diagram in fig. 4d shows that the tumour developed highly irregular contour only in the case of slowly moving front (*i.e.* small chemotactic coefficient and proliferation), since for fast moving front the characteristic mode decrease, until only $\ell = 1$ is unstable.

Moreover, it is interesting to consider the role played by the radius of the growing tumour in the development of instabilities, while keeping all the other parameters fixed (see fig. 5). Figure 5a reports the results for a set of parameters R_{out}, R_N, β and σ for which, independently from R_T, the most unstable mode is always $\ell = 1$. This situation corresponds to a sort of translation of the spheroid inside the domain (see fig. 5a on the right). On the other hand, the characteristic mode depends on the MCTS size in a certain range of material parameters (see fig. 5b). Indeed, it increases for increasing R_T, so that bigger tu-

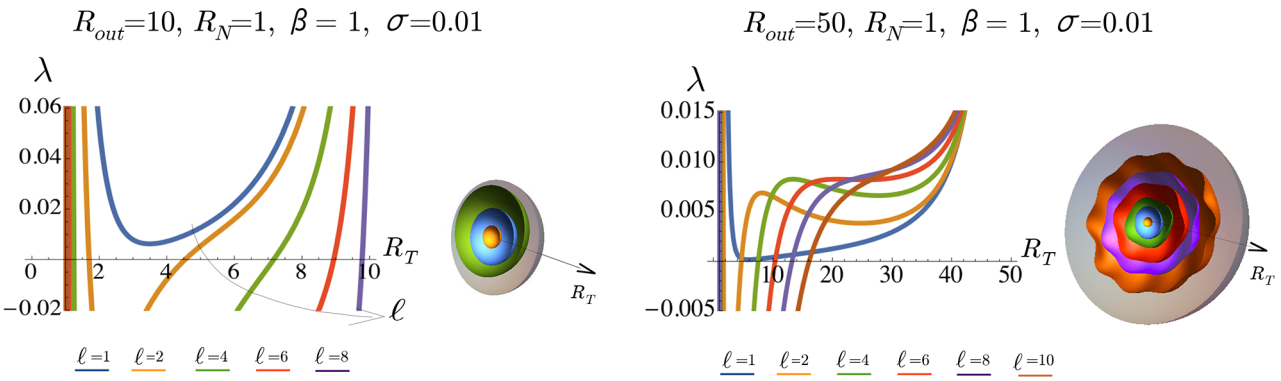

Fig. 5. Evolution of the time growth rate of the perturbation λ with respect to the dimensionless tumour radius, R_T, for different values of ℓ (with $\ell = 1, 2, 4, 6, 8, 10$). (a) For the chosen set of parameters, $\ell = 1$ is the most unstable mode, whatever the tumour radius is. The deformed shapes corresponding to $R_T = 2, 5, 8$ are reported aside (the gray region represents the outer environment). (b) The characteristic mode ℓ changes for different values of the tumour radius. Aside the dispersion curves, the section of the tumour perturbed shapes are reported for $R_T = 2.5, 8, 12.5, 20, 26, 35$ to which the corresponding characteristic modes are $\ell = 1, 2, 4, 6, 8, 10$, respectively.

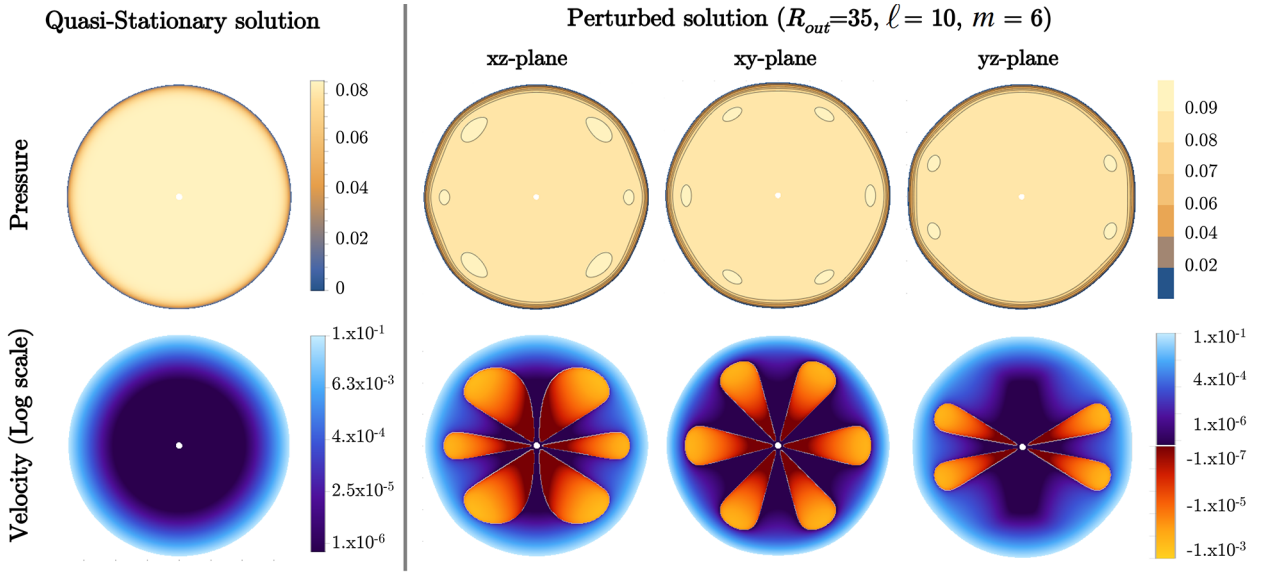

Fig. 6. Evolution of the quasi-stationary and perturbed pressure and velocity fields for $R_n = 1$, $R_T^* = 35$, $R_{\text{out}} = 50$ for a perturbation of the kind $e^{\lambda t} Y_{10}^6(\theta, \varphi)$. Since higher changes in the velocity and pressure field occur only at the interface, we use a logarithmic scale in the velocity plot in order to show small variations of the perturbed field inside the bulk of the tumour. The perturbed velocity field highlights the existence of negative radial velocities (*i.e.* radial convergent flow), as pointed out in [66, 67].

mours show more irregularities at their border. Therefore, a growing MCTS can undergo a morphological transition that may significantly affect the invasion pattern towards the typical finger-like structures observed for invasive carcinomas (see fig. 5b).

Finally, fig. 6 depicts the perturbed pressure and velocity fields for a linearly unstable perturbation, given by a spherical harmonic of the kind $Y_{10}^6(\theta, \varphi)$. The highest variation of the pressure is located in a thin shell closer to the interface of the tumour, so that in the bulk of the tumour the velocity is almost null. In the region just at the rear of small protrusions (due to the perturbation of the boundary), the pressure field increases, so that the velocity at the border of the MCTS where a protrusion form, for the unstable modes (such as the one reported in fig. 6), is higher than the velocity in the invagination on the contour. Furthermore, from the perturbed field it is possible to appreciate small negative radial velocities in the bulk, just at the rear of the region where protrusion forms. Thus, while the spheroid surface moves outward, some cells inside the cluster move inward. This result confirms the existence of a radial convergent flow, in addition to the divergent flow that makes the aggregate expand, as pointed out in [66, 67]. This effect combined with the higher velocity associated to the protrusion border could explain the possible detachment of carcinoma cells that lead to metastasis and thus the higher invasivity of tumours with irregular contours.

Even though the onset of irregular contours and the development of a retrograde flow are in qualitative agreement with biological experiments [66–68], a direct quantitative comparison between our predictions and the biological experiments is not straightforward. First, not all the data required by the mathematical model, even though measurable in principle, are reported in the literature. Second, most of the work in the vast literature on MCTSs focus on the effect of nutrients availability and stress on the growth of the spherical tumour aggregate, whereas little attention has been paid to the systematic mapping of contour instabilities onset and evolution. Therefore, further morphological data on MCTS, combined with estimates of the underlying biological parameters involved in the process (*i.e.* nutrients diffusion and uptake, surface tension of the aggregate and permeability of the porous medium), are highly required for the future validation of the proposed model.

5 Conclusions

In this work we have presented a continuum model for describing the avascular growth of a multicellular tumour spheroid, comprising a fixed necrotic core surrounded by a region of proliferative cells, guided by the uptake of a diffusing nutrient. The proposed model encapsulates the diffusion of a chemical species from the vasculature of the healthy region and the tumour cell response to nutrients, via their proliferation and their chemotactic migration inside the extracellular space. The proposed model differs from existing approaches [2, 49, 50] since it considers a growth though a rigid, porous surrounding material. Moreover, the MCTS expansion is guided not only by cell proliferation as in [2, 49, 50], but also by the chemotactic motion of cells, through a non-convective mass flux term. Differently from [2, 50], that assumed a Gibbs-Thompson relation [69] on the moving boundary for the chemical potential, we considered a mechanical effect in term of a surface tension at the MCTS outer boundary, leading to the Young-Laplace equation at the interface.

The proposed model is governed by five dimensionless parameters: two of them, β and σ are called motility parameters and representing the mechano-biology cues, the other three are denoted size parameters and are related to the typical sizes of the domains with respect to the diffusive length. The analytic results predicted the existence of a quasi-stationary radially symmetric tumour configuration that is always linearly unstable to asymmetric perturbations involving spherical harmonics $Y_\ell^m(\theta, \phi)$, with the range of the unstable modes depending on the dimension of the domain with respect to the diffusive length and on the motility parameter β, related to the chemotactic growth of the tumour. We remark that, whilst a MCTS growing inside an infinite homogeneous domain is marginally stable, *i.e.* $\lambda = 0$ for $\ell = 1$ [11, 15, 50], the proposed model is always linearly unstable, since translational symmetry is broken by considering a finite dimension of the surrounding media. Furthermore, differently from existing works [2, 8, 9, 14, 15, 17], the perturbation analysis is conducted here without neglecting the diffusion timescale in the unstable growth rate.

The analysis of the perturbed field also pointed out a possible mechanism that could lead to the detachment of metastasis from the primary tumour mass, based on the development of higher velocity at the border of the MCTS and a convergent flow inside where protrusions form. This mechanism could explain the reason why the propensity for asymmetric invasion and the installation of irregular morphology characterize the growth of aggressive carcinomas *in vivo*. Thus, this approach has the potential to foster our understanding on the process of transition from the benign to the aggressive tumour stage and might provide also some indications for improving therapeutic treatments. Indeed, more blurred and irregular contours detected *in vivo* can be related to more malignant tumour, with respect to smoother and clearer contours that can be associated to benign carcinomas.

However, the present model considers a really simplified geometry and adopts some simplifications in order to obtain a model that can be studied analytically. Thus, future improvements of the proposed mathematical model should focus on the explicit description of the quiescent cell region (that in the present model corresponds to the region of the spheroid in which we have an almost null velocity) and on tracking the evolution of the inner necrotic core, occurring, for instance, when the nutrients concentration attains a specific value [2, 12] (whereas in the present work the fixed radius R_N of the necrotic core is a parameter in the sensitivity analysis). Then, the stability analysis can be enriched by considering the weakly nonlinear interactions of the asymmetric modes, as well as their evolution depending on the order m of the spherical harmonic perturbation (as done for example in [15] in a simplified case) and numerical techniques should be developed in order to simulate the fully nonlinear evolution of the morphological transition.

From the modelling point of view, future studies should also consider the effect of the cells populating the surrounding healthy environment on the consumption of nutrients and the effect of varying local densities (both inside the healthy tissue and inside the different tumour regions) on the nutrient diffusion coefficient. Then, the effect of solid mechanical stresses on the growth dynamics of tumours [32, 61, 67, 70–73] and the effect of the possible deformation, degradation and reorganization of extracellular matrix fibres [74–76] should be included to move towards a more realistic representation of the problem. Indeed, for tumours growing both *in vivo* and in xenograft animal models, the description of the system evolution is far more complex than the one proposed in this work, referred to MCTS growth inside inert and rigid ECM scaffolds. In particular, it has been shown that the geometrical and mechanical properties of the ECM [74, 75] play an important role for the possible formation of metastasis, since they can lead to growth arrest (*i.e.* spheroid compartmentalization) or, on the contrary, foster the detachment of invasive cells. Along with the rigidity of the matrix, its density, and the tensile forces generated in the ECM [74, 75], more recent studies identify the matrix pore size as the

critical property modulating cancer cell invasion [77, 78]. Based on these biological observations, some recent mathematical models have been developed to take into account, on the one hand, MCTS segregation by thick porous (but still rigid and homogeneous) structures [79–81] and, on the other, ECM deformation [82]. Furthermore, not only ECM fibers can accumulate or being degraded at the host-MCTS interface, but they strongly reorganize, aligning parallel to the tumour border, in a first stage, and then perpendicular to the tumour boundary [74].

Thus, to take into account all these aspects and more realistically describe tumour growth *in vivo*, an anisotropic poro-elasto-visco-plastic model with a threshold (based on microscopic arguments) for cell motion should be developed. However in that case tumour irregular contours will likely arise for inhomogeneity and anisotropy in the ECM, whereas this work demonstrates that mechano-biological and (macroscopic) geometrical cues can determine the occurrence of a morphological transition in growing tumours that can promote invasiveness, even in a homogeneous environment. The theoretical results push towards the developments of further biological experiments for accurate characterization of MCTS morphology and careful measures of the surface tension and the interstitial pressure within MCTSs [59,83], as well as growth and mobility properties of the tumour cells to validate the predictions of the model. Indeed, the integration of mathematical tools in biological research could be crucial for estimating the tumour's ability to invade its host environment.

This work was funded by the "Associazione Italiana per la Ricerca sul Cancro" (AIRC) through My First AIRC Grant 17412, partially supported by the "Start-up Packages and PhD Program" project, co-funded by Regione Lombardia through the "Fondo per lo sviluppo e la coesione 2007-2013-formerly FAS", and by the "Progetto Giovani GNFM 2016".

References

1. J. Folkman, M. Hochberg, J. Exp. Med. **138**, 745 (1973).
2. H. Byrne, M. Chaplain, Eur. J. Appl. Math. **6**, 639 (1997).
3. R. Sutherland, R. Durand, in *Spheroids in Cancer Research*, edited by H. Acker, J. Carlsson, R. Durand, R.M. Sutherland, Vol. **95** of *Recent Results in Cancer Research* (Springer, Berlin, Heidelberg, 1984) pp. 24–49.
4. K. Groebe, W. Mueller-Klieser, Eur. Biophys. J. **19**, 169 (1991).
5. R. Sutherland, Science **240**, 177 (1988).
6. J. Folkman, Adv. Cancer Res. **19**, 331 (1974).
7. V.R. Muthukarruppan, L. Kubai, R. Auerbach, J. Natl. Cancer Inst. **69**, 699 (1982).
8. J.A. Adam, Math. Biosci. **81**, 229 (1986).
9. J.A. Adam, Math. Biosci. **86**, 183 (1987).
10. J.A. Adam, S.A. Maggelakis, Bull. Math. Biol. **52**, 549 (1990).
11. H. Byrne, M.A.J. Chaplain, Math. Biosci. **130**, 151 (1995).
12. H. Byrne, M.A.J. Chaplain, Math. Biosci. **135**, 187 (1996).
13. M.A.J. Chaplain, *Experimental and Theoretical Advances in Biological Pattern Formation*, chapter *The development of a spatial pattern in a model for cancer growth* (Plenum Press, 1993) pp. 45–60.
14. H.P. Greenspan, Studies Appl. Math. **52**, 317 (1972).
15. H. Byrne, J. Math. Biol. **39**, 59 (1999).
16. S.A. Maggelakis, J.A. Adam, Math. Comput. Modell. **13**, 23 (1990).
17. D.L.S. McElwain, L.E. Morris, Math. Biosci. **39**, 147 (1978).
18. D. Ambrosi, L. Preziosi, Math. Models Methods Appl. Sci. **12**, 737 (2002).
19. R.P. Araujo, D.L.S. McElwain, Bull. Math. Biol. **66**, 1039 (2004).
20. J.S. Lowengrub, H.B. Frieboes, F. Jin, Y.L. Chuang, X. Li, P. Macklin, S.M. Wise, V. Cristini, Nonlinearity **23**, R1 (2010).
21. D. McElwain, G. Pettet, Bull. Math. Biol. **55**, 655 (1993).
22. C. Chen, H. Byrne, J. King, J. Math. Biol. **43**, 191 (2001).
23. K.A. Landman, C.P. Please, Math. Med. Biol. **18**, 131 (2001).
24. M. Steinberg, Science **141**, 401 (1963).
25. R. Foty, G. Forgacs, C. Pflegerand, M. Steinberg, Phys. Rev. Lett. **72**, 2298 (1994).
26. G. Forgacs, R. Foty, Y. Shafrir, M. Steinberg, Biophys. J. **74**, 2227 (1998).
27. G. Vitale, L. Preziosi, Math. Models Methods Appl. Sci. **21**, 1901 (2011).
28. M.A.J. Chaplain, B.D. Sleeman, J. Math. Biol. **31**, 431 (1993).
29. R. Skalak, S. Zargaryan, R.K. Jain, P.A. Netti, A. Hoger, J. Math. Biol. **34**, 889 (1996).
30. D. Ambrosi, F. Mollica, J. Math. Biol. **48**, 477 (2004).
31. T. Roose, P.A. Netti, L.L. Munn, Y. Boucher, R.K. Jain, Microvasc. Res. **66**, 204 (2003).
32. C. Voutouri, F. Mpekris, P. Papageorgis, A. Odysseos, T. Stylianopoulos, PLoS ONE **9**, e104717 (2014).
33. R. Vandiver, A. Goriely, J. Biol. Dyn. **3**, 180 (2009).
34. T. Stylianopoulos, J.D. Martin, V.P. Chauhan, S.R. Jain, B. Diop-Frimpong, N. Bardeesy, B.L. Smith, C.R. Ferrone, F.J. Hornicek, Y. Boucher, L.L. Munn, R.K. Jain, Proc. Natl. Acad. Sci. U.S.A. **109**, 15101 (2012).
35. D. Ambrosi, L. Preziosi, Biomech. Model. Mechanobiol. **8**, 397 (2009).
36. D. Ambrosi, L. Preziosi, G. Vitale, Mech. Res. Commun. **42**, 87 (2012).
37. C. Giverso, M. Scianna, A. Grillo, Mech. Res. Commun. **68**, 31 (2015).
38. B. Aigouy, R. Farhadifar, D. Staple, A. Sagner, J. Röper, F. Jülicher, S. Eaton, Cell **142**, 773 (2010).
39. T. Vasilica Stirbat, S. Tlili, T. Houver, J.P. Rieu, C. Barentin, H. Delanoë-Ayari, Eur. Phys. J. E **36**, 84 (2013).
40. J. Ranft, M. Basan, J. Elgeti, J. Joanny, J. Prost, F. Jülicher, Proc. Natl. Acad. Sci. U.S.A. **107**, 20863 (2010).
41. J.J. Casciari, S.V. Sotirchos, R.M. Sutherland, Cell Prolif. **25**, 1 (1992).
42. M. Marusic, Z. Bajzer, J.P. Freyer, S. Vuk-Pavlovic, Cell Prolif. **27**, 73 (1994).
43. R. Muir, *Muir's Textbook of Pathology*, 15th edition (CRC Press, 2012).

44. S.S. Cross, D.W.K. Cotton, J. Pathol. **166**, 409 (1992).
45. S.S. Cross, J.P. Bury, P.B. Silcocks, T.J. Stephenson, D.W.K. Cotton, J. Pathol. **172**, 317 (1994).
46. G. Landini, J.W. Rippin, J. Pathol. **179**, 210 (1996).
47. R. Sutherland, R.E. Durand, Int. J. Radiat. Biol. **23**, 235 (1973).
48. M. Tubiana, Brit. J. Radiol. **44**, 325 (1971).
49. H.P. Greenspan, J. Theor. Biol. **56**, 229 (1976).
50. H. Byrne, M. Chaplain, Math. Comput. Model. **24**, 1 (1996).
51. M. Espinosa, G. Ceballos-Cancino, R. Callaghan, V. Maldonado, N. Patiño, V. Ruíz, J. Meléndez-Zajgla, Cancer Lett. **318**, 61 (2012).
52. A. Nyga, U. Cheema, M. Loizidou, J. Cell Commun. Signal. **5**, 239 (2011).
53. S. Wise, J. Lowengrub, H. Frieboes, V. Cristini, J. Theor. Biol. **253**, 524 (2008).
54. A. Ramanathan, C. Wang, S. Schreiber, Proc. Natl. Acad. Sci. U.S.A. **102**, 992 (2005).
55. H. Byrne, L. Preziosi, Math. Med. Biol. **20**, 341 (2003).
56. K.J. Painter, Bull. Math. Biol. **71**, 1117 (2009).
57. E.T. Roussos, J.S. Condeelis, A. Patsialou, Nat. Rev. Cancer **11**, 573 (2011).
58. E. Keller, L. Segel, J. Theor. Biol. **30**, 225 (1971).
59. A. Fathi-Azarbayjani, A. Jouyban, Bioimpacts **5**, 29 (2015).
60. T. Stirbat, A. Mgharbel, S. Bodennec, K. Ferri, H. Mertani, J.-P. Rieu, H. Delanoë-Ayari, PLoS ONE **8**, e52554 (2013).
61. G. Helmlinger, P.A. Netti, H.C. Lichtenbeld, R.J. Melder, R.K. Jain, Nat. Biotechnol. **15**, 778 (1997).
62. A. Nayfeh, *Perturbation Methods* (John Wiley and Sons, 2000).
63. P. Ciarletta, Eur. Biophys. J. **41**, 681 (2012).
64. C. Giverso, M. Verani, P. Ciarletta, J. R. Soc. Interface **12**, 20141290 (2015).
65. C. Giverso, M. Verani, P. Ciarletta, Biomech. Model. Mechanobiol. **15**, 643 (2015).
66. M. Dorie, R. Kallman, D. Rapacchietta, D. Van Antwerp, Y. Huang, Exp. Cell Res. **141**, 201 (1982).
67. M. Delarue, F. Montel, O. Caen, J. Elgeti, J.M. Siaugue, D. Vignjevic, J. Prost, J.F. Joanny, G. Cappello, Phys. Rev. Lett. **110**, 138103 (2013).
68. H. Frieboes, X. Zheng, C.-H. Sun, B. Tromberg, R. Gatenby, V. Cristini, Cancer Res. **66**, 1597 (2006).
69. J. Langer, Rev. Mod. Phys. **52**, 1 (1980).
70. G. Cheng, J. Tse, R. Jain, L. Munn, PLoS ONE **4**, e4632 (2009).
71. F. Montel, M. Delarue, J. Elgeti, L. Malaquin, M. Basan, T. Risler, B. Cabane, D. Vignjević, J. Prost, G. Cappello, J.F. Joanny, Phys. Rev. Lett. **107**, 188102 (2011).
72. K. Alessandri, B.R. Sarangi, V.V. Gurchenkov, B. Sinha, T.R. Kießling, L. Fetler, F. Rico, S. Scheuring, C. Lamaze, A. Simon, S. Geraldo, D. Vignjević, H. Doméjean, L. Rolland, A. Funfak, J. Bibette, N. Bremond, P. Nassoy, Proc. Natl. Acad. Sci. U.S.A. **110**, 14843 (2013).
73. R.K. Jain, J.D. Martin, T. Stylianopoulos, Annu. Rev. Biomed. Engin. **16**, 321 (2014).
74. K. Kopanska, Y. Alcheikh, R. Staneva, D. Vignjevic, T. Betz, PLoS ONE **11**, e0156442 (2016).
75. P. Provenzano, K. Eliceiri, J. Campbell, D. Inman, J. White, P. Keely, BMC Med **4**, 38 (2006).
76. L. Kaufman, C. Brangwynne, K. Kasza, E. Filippidi, V. Gordon, T. Deisboeck, D. Weitz, Biophys. J. **89**, 635 (2005).
77. K. Wolf, M. Te Lindert, M. Krause, S. Alexander, J. Te Riet, A. Willis, R. Hoffman, C. Figdor, S. Weiss, P. Friedl, J. Cell Biol. **201**, 1069 (2013).
78. A. Haeger, M. Krause, K. Wolf, P. Friedl, Biochim. Biophys. Acta **1840**, 2386 (2014).
79. C. Giverso, A. Grillo, L. Preziosi, Biomech. Model. Mechanobiol. **13**, 481 (2014).
80. A. Arduino, L. Preziosi, Int. J. Non-Linear Mech. **75**, 22 (2015).
81. C. Giverso, A. Arduino, L. Preziosi, "How Nucleus Mechanics and ECM Microstructure Influence the Invasion of Single Cells and Multicellular Aggregates," submitted (2016).
82. G. Sciumé, R. Santagiuliana, M. Ferrari, P. Decuzzi, B. Schrefler, Phys. Biol. **11**, 065004 (2014).
83. R.K. Jain, Sci. Am. **271**, 58 (1994).